stability of the complex formed by major histocompatibility complex molecules, altered peptide ligands and T-cell receptors (MHC – altered-peptide-ligand – TCR complex) as recently shown for the altered AH1 tumor peptide, for which increased MHC – peptide – TCR complex stability was correlated with improved immune response.[17] Alternatively, perhaps a T-cell antagonist is converted into an agonist by repair of TCR – peptide – MHC interface defects, as suggested by other research groups.[18]

Herein we were able to correlate immunogenicity (particularly protective efficacy of a synthetic peptide in vivo) with three-dimensional structural features. Understanding the structure-protection relationship will lead to a more rational design of a *P. falciparum* malaria vaccine in the near future and any one of the reported modified peptides could be used as part of a multicomponent subunit malaria vaccine.

Received: June 12, 2001
Revised: October 10, 2001 [Z17274]

[1] K. Marsh, *Parasitology* **1992**, *104*, 553 – 569.
[2] L. H. Miller, M. F. Good, G. Milon, *Science* **1994**, *264*, 878 – 1883.
[3] H. D. Engers, T. Godal, *Parasitol. Today* **1998**, *4*, 56 – 64.
[4] P. Graves, H. Gelband, P. Garner, *Parasitol. Today* **1998**, 219 – 221.
[5] L. H. Miller, S. L. Hoffman, *Nature Med. Vaccine Suppl.* **1998**, *4*, 520 – 524.
[6] A. A. Holder, M. J. Blackman, *Parasitol. Today* **1994**, *10*, 182 – 184.
[7] M. Urquiza, L. E. Rodriguez, J. E. Suarez, F. Guzman, M. Ocampo, H. Curtidor, C. Segura, E. Trujillo, M. E. Patarroyo, *Parasite Immunol.* **1996**, *18*, 515 – 526.
[8] M. Plebanski, A. V. S. Hill, *Curr. Opin. Immunol.* **2000**, *12*, 437 – 441.
[9] M. Aidoo, V. Udhayakumar, *Parasitol. Today* **2000**, *16*, 50 – 56.
[10] L. E. Rodriguez, M. Urquiza, M. Ocampo, J. Suarez, H. Curtidor, F. Guzman, L. E. Vargas, M. Triviños, M. Rosas, M. E. Patarroyo, *Parasitology* **2000**, *120*, 225 – 235.
[11] E. Lioy, J. Suarez, F. Guzman, S. Siegrist, G. Pluschke, M. E. Patarroyo, *Angew. Chem.* **2001**, *113*, 2701 – 2706; *Angew Chem. Int. Ed.* **2001**, *40*, 2631 – 2635.
[12] R. A. Houghten, *Proc. Natl. Acad. Sci. USA* **1985**, *82*, 5131 – 5139.
[13] R. Rodriguez, A. Moreno, F. Guzman, M. Calvo, M. E. Patarroyo, *Am. J. Trop. Med. Hyg.* **1990**, *43*, 339 – 354.
[14] V. Waterhouse, C. Johnson, *Biochemistry* **1994**, *33*, 2121 – 2128.
[15] K. Wüthrich, *NMR of Protein and Nucleic Acids*, Wiley, New York, **1986**.
[16] R. A. Laskowski, M. W. MacArthur, D. S. Moss, J. M. Thorton, *J. Appl. Crystallogr.* **1993**, *26*, 283 – 291.
[17] J. E. Slanky, F. M. Rattis, L. F. Boyd, T. Famhy, E. M. Jaffe, J. Schenk, D. M. Pardoll, *Immunity* **2000**, *13*, 529 – 583.
[18] B. M. Baker, S. J. Gagnon, W. Biddison, D. C. Willey, *Immunity* **2000**, 475 – 484.

## β-Fibrillogenesis from Rigid-Rod β-Barrels: Hierarchical Preorganization Beyond Microns**

Gopal Das, Lahoussine Ouali, Marc Adrian, Bodo Baumeister, Kevin J. Wilkinson, and Stefan Matile*

Fibrillogenesis of β-sheet peptides is attracting considerable scientific attention because of its importance in medicine and nanoscience.[1–12] Recent structural studies with synthetic models go beyond pure peptide chemistry.[5–9] These studies were consistently in support of repeated "β-dyads" of polar and apolar amino acid residues as the minimal structural requirement for β-fibrillogenesis[4] (if any),[3] and also supported a universal "cross-β" motif in β-fibrillar quaternary structures. The term cross-β is used for layered β-strands that are oriented perpendicular to the long fibril axis. In this case, one fibril (or protofilament) dimension is defined by the length of the β-strand, the other by the number of stacked, amphiphilic β-bilayers.[1–12] Further self-assembly of β-fibrils produces a quite remarkable, in part transient, polymorphism including formation of helices, ribbons, tubes, and sheets.[1–12] Whereas elegant strategies to inhibit random β-fibril self-assembly[8, 9] and to control two-dimensional organization of β-sheet monolayers[13] have been conceived recently, little is known about how to direct fibril self-assembly toward higher order structures. However, the difficulties with preorganizing β-sheet tertiary structures can be bypassed by using *p*-oligophenyl rods instead of β-sheets as β-barrel "staves".[14–16] The objective of this study was to expand this powerful preorganization strategy from tertiary β-barrel structures to quaternary β-fibril structures. We report, for the first time, the direct observation of "rigid-rod" β-barrels by atomic force microscopy as well as their controlled transformation into unidirectional self-assembled "rigid-rod" β-fibrils of exceptional beauty.

The formation of tetrameric rigid-rod β-barrels **1** is preorganized by rigid-rod "staves" in the monomers **2** (Figure 1). Barrel – stave supramolecule **1** further contains 32 interdigitating β-dyad-pentapeptides that produce hydrophobic outer and hydrophilic inner β-barrel surfaces (Figure 1).[14–16] Structural and functional studies implied that tetramer **1**

[*] Prof. S. Matile, Dr. G. Das, Dipl.-Chem. B. Baumeister
Department of Organic Chemistry
University of Geneva
1211 Geneva (Switzerland)
Fax: (+41) 4122-328-7396
E-mail: stefan.matile@chiorg.unige.ch
Dr. L. Ouali, Dr. K. J. Wilkinson
Analytical and Biophysical Environmental Chemistry (CABE)
University of Geneva, 1211 Geneva (Switzerland)
Dr. M. Adrian
Laboratoire d'Analyse Ultrasructurale (LAU)
Bâtiment de Biologie
Université de Lausanne, 1015 Lausanne (Switzerland)

[**] We thank J. Buffle and J. Dubochet for their fruitful discussions and the Swiss NSF (21-57059.99 (S.M.), 2000-050629.97 (K.J.W.), and the National Research Program "Supramolecular Functional Materials" 4047-057496 (S.M.)) for their financial support.

  1433-7851/01/4024-4657 $ 17.50+.50/0 

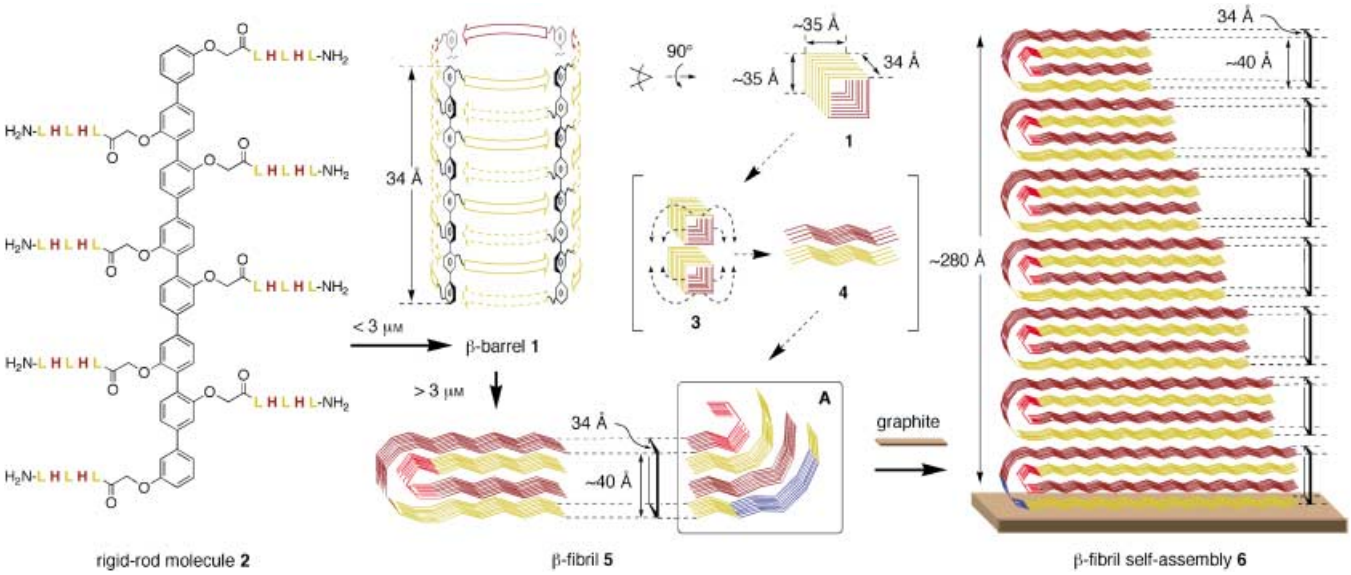


Figure 1. Hierarchical preorganization of tertiary (β-barrel **1**) and tentative quaternary structures (β-fibril **5** and β-fibril heptamer **6**) by rigid-rod molecule **2**. Amino acid residues (one-letter abbreviation, **2**) are in yellow (hydrophobic) and bronze (hydrophilic). β-Strands are depicted with an identical color code, either as arrows pointing to the C-terminus (**1**) or as lines (**1**, **3**–**6**). β-Barrel turns are in red, and fibril curvature induced by surface repulsion in blue. Tentative (transient) structures (and mechanisms) are in brackets (**3**,**4**), frames (A), and dashed arrows. The indicated dimensions are estimates that are compatible with literature[1–12] and experimental values (Figures 2, 4, and 5). The presence of a contracted trimer existing presumably in a pH-dependent equilibrium with tetramer **1** is not shown for clarity.[16]

forms, as expected, in lipid bilayers and, more surprisingly, in water.[16, 17] This previously suspected, but somewhat counterintuitive, formation of rigid-rod β-barrels with hydrophobic exteriors in water is here confirmed at relevant concentrations (< 3 μM, see below) by using atomic force microscopy (AFM). AFM images were obtained by adsorption of β-barrels **1** from dilute aqueous solutions onto mica (Figure 2).

Most of the detected objects have heights that match the length of the *p*-octiphenyl barrel staves within the vertical image resolution of 1.0–2.0 Å[11, 18] (Figure 2A); control experiments unambiguously confirmed that the additional, much smaller "objects" originate from residual 2-(4-morpholinyl)ethanesulfonic acid (MES) buffer. Consistent with the similarity between the diameter and height of tetramer **1** (Figure 1), the significant objects, within the poorer lateral AFM image resolution, had identical mean widths around 40 Å (Figure 2A). Although orientation of the barrels in the vertical direction is expected from interactions of hydrophilic barrel ends (rather than hydrophobic barrel sides) with the hydrophilic mica, no conclusions can be reached concerning the barrel orientation from the AFM images depicted in Figure 2. A conelike rather than a cylindrical barrel shape, without central channels, appeared in surface plots (Figure 2C). This appearance corresponds exactly, however, to the image distortion that is anticipated for scanning with commercial AFM tips with a radius of curvature of approximately 10 nm[6] without further refinements such as tip screening and image averaging.[18]

Rigid-rod β-barrels **1** were as poorly soluble in water as one would expect on the basis of their hydrophobic sides.[14–16] Transformation of β-barrels into β-fibrillar quaternary structures occured at around saturation but before the appearance of turbidity. β-Fibrillogenesis was characterized with thioflavin T (ThT), an amyloid-specific fluorophore (Figure 3).[5]

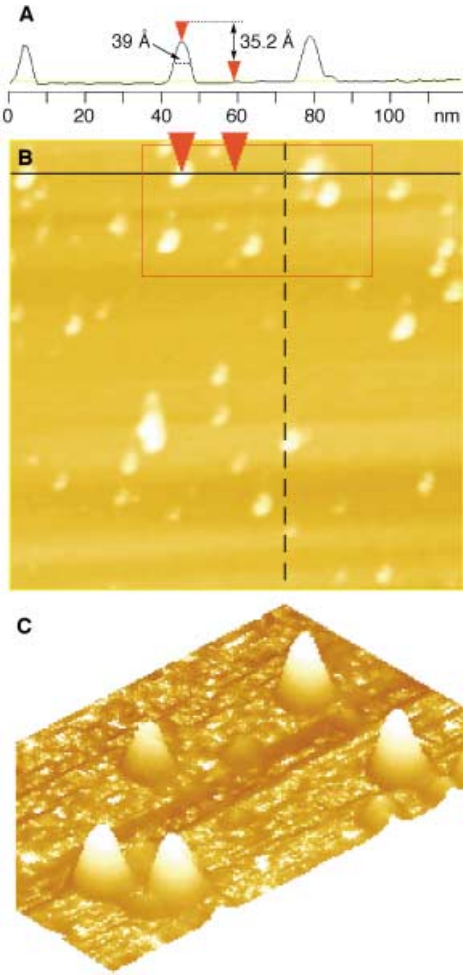


Figure 2. AFM image of rigid-rod β-barrels **1** on mica (1.5 μM **2**, 1.0 mM MES, pH 5.5). A) Heights and widths for β-barrels centered on the solid black line in (B); C) surface plot of the area within the frame in (B).

  1433-7851/01/4024-4658 $ 17.50+.50/0 

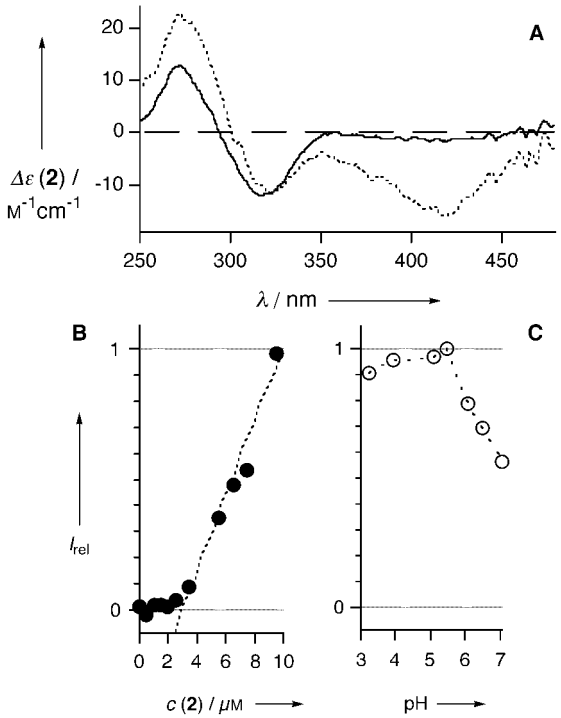


Figure 3. β-Fibrillogenesis from rigid-rod β-barrels **1** characterized by the thioflavin T (ThT) binding assay.[5] A) Circular dichroism (CD) spectra of rigid-rod β-fibrils (5 μM **2**, 10 mM MES, pH 5.5) in the presence (dotted line) and absence (solid line) of ThT (10 μM). B) and C) Changes in the spectroscopic properties of ThT observed by CD (see example in A), fluorescence emission (intensity shown for $\lambda_{ex} = 420$ nm, $\lambda_{em} = 500$ nm), and FRET (intensity at $\lambda_{ex} = 319$ nm, $\lambda_{em} = 500$ nm (depicted) as a function of *p*-octaphenyl concentration (B, pH 5.5) and pH (C, 5 μM **2**).

The appearance of a broad, induced CD Cotton effect (ICD CE) centered at 420 nm was observed in the circular dichroism (CD) spectra of *p*-octiphenyl[14–16] β-fibrils (Figure 3A, solid line) upon addition of ThT (Figure 3A, dotted line). This ICD CE demonstrated the location of ThT chormophores within the chiral environment provided by rigid-rod β-fibrils. The binding of ThT to rigid-rod β-fibrils was further observable by the characteristic increase in ThT emission.[1–12] The presence of ThT emission upon excitation of *p*-octiphenyl rods (319 nm) rather than ThT itself (420 nm) was indicative of fluorescence resonance energy transfer (FRET) from *p*-octiphenyl donors to ThT acceptors. The presence of FRET provided further corroborative evidence for ThT binding to rigid-rod β-fibrils since it operates over short distances only.

The properties of rigid-rod β-fibrils could thus be readily identified from the ICD CE, emission, or FRET related to the ThT fluorophore. The dependence of ThT binding on the concentration of rod **2** suggested that β-fibrillogenesis occurs above a critical barrel concentration $c = 3$ μM (Figure 3B). Maximal β-fibrillogenesis was observed at pH 5.5 (Figure 3C).[16] As for β-amyloid fibrils,[8, 9] this finding suggested intermolecular interactions between protonated and neutral histidines in rigid-rod β-fibrils.

Direct observation of hydrated rigid-rod β-fibrils was possible by using electron cryomicroscopy and cryonegative staining.[12, 19] This method was of interest because it provides access to high-contrast cryomicrographs of intact vitrified structures. Rigid-rod β-fibrils appear white against a background with an enhanced darkness from ammonium molybdate (Figure 4).[12, 19]

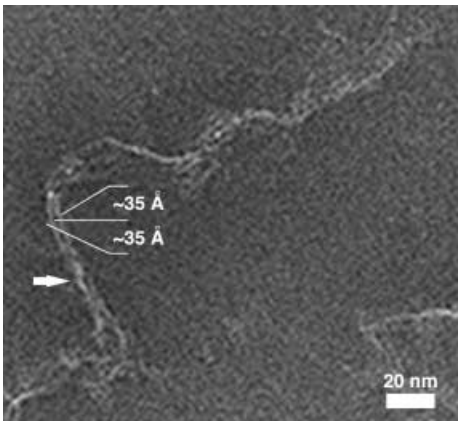


Figure 4. Electron cryomicrograph of rigid-rod β-fibrils (15 μM **2**, 10 mM MES, pH 5.5). Apparent fibril dimensions ca. $3.5 \times 3.5$ nm (for tentative structure, see **5** in Figure 1) and a fibril crossover (arrow) are indicated.

Short, fibrillar quaternary structures of about uniform diameter near the resolution limit (ca. $3.5 \times 3.5$ nm) were observed at pH 5.5 (Figure 3C and Figure 4). These "rod-like"[12] fibrils self-assembled in a poorly organized manner and included rare fibril crossovers (Figure 4, arrow). Their highly variable overall appearance included some indications of unidirectional fibril self-assembly into meandering, "ribbonlike" quaternary structures and a few less structured, presumably nonfibrillar, subdomains. Some of the vitrified "rigid-rod" β-fibrils were similar to intermediate rather than mature amyloid-β-fibrils.[12] This similarity may be of potential interest because of the likely "noncross-β" structure of rigid-rod β-fibrils (Figure 1, see below). Consistent with increased β-bilayer charge and hydrophobicity upon full histidine protonation and deprotonation, much shorter "mini-fibrils" and amorphous aggregates were detected at pH 4.5 and 6.5, respectively (not shown).

The overall poor self-organization of dilute aqueous rigid-rod β-fibrils was dramatically amplified on graphite. Indeed, AFM images of rigid-rod β-fibrils revealed hierarchical preorganization beyond the micron scale in three dimensions (Figure 5).

β-Fibril self-assemblies on graphite are composed of fibrils with uniform width and height of about 4.0 nm (Figure 5, bottom). Similar fibril dimensions were identified in assemblies observed by using electron cryomicroscopy (Figure 4). A uniform height of approximately 28.0 nm for the assemblies suggests that about seven of these β-fibrils grow one on top of the other, without any irregularities, even at the termini (Figure 5, top). β-Fibril heptamers are further characterized by extensive meandering with some "U-turns" that create lateral, often loose, contact between two β-fibril heptamers. "Dimeric" β-fibril heptamers, however, never cross, twist, touch, or fuse.

Although speculations on possible structures of rigid-rod β-fibrils and β-fibril self-assemblies need appropriate reservation,[1–12] some comments may be constructive for future

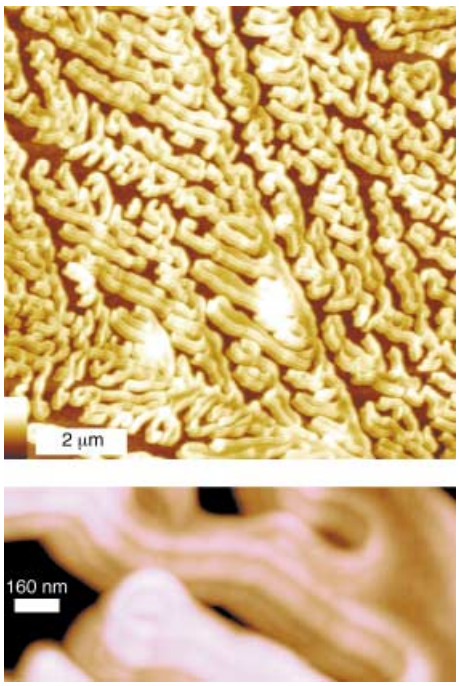


Figure 5. AFM image of rigid-rod β-fibril self-assemblies on graphite at low (top, vertical scale bar = 80 nm) and high magnification (bottom, 5 μM **2**, 3.3 mM MES, pH 5.5; for tentative structure, see **6** in Figure 1).

developments (Figure 1). With direct structural evidence for rigid-rod β-barrels **1** in hand (Figure 2), it is reasonable to propose that β-fibrillogenesis is initiated above the critical barrel concentration of $c = 3\ \mu M$ by lateral barrel–barrel contacts between hydrophobic β-faces. Under these partially denaturating conditions,[1–12] β-barrel dimers **3** (or higher oligomers) may transform into transient β-bilayers **4**. Dimerization of β-bilayers **4**, perhaps directed by β-barrel turns (Figure 1, red), gives the tentative rigid-rod β-fibril **5**. Note that in contrast to classical dimeric β-bilayers,[1–12] β-fibril **5** comprises a "noncross-β" motif and, perhaps, terminal and some central β-barrel turns. Dimensions of $3.4 \times$ ca. 4.0 nm estimated for β-fibril **5** roughly match experimental values (Figure 4 and 5). Initiation and termination of unidirectional self-assembly of β-fibril **5** into heptamer **6** (Figure 5) is then similarly preorganized by (transient) nucleating β-barrel turns (Figure 1A, red) and further supported by surface repulsion (Figure 1A, blue). Note that twisting of single fibrils in the tentative heptamer **6** cannot be excluded experimentally.

In conclusion, this report on hierarchical preorganization of β-sheet structures by synthetic rigid-rod "β-dyad" peptides describes a rich tertiary and quaternary structural plasticity of delightful order and beauty. Unprecedented direct structural evidence at the tertiary structural level will increase confidence in efforts to exploit the easily accessible functional plasticity of rigid-rod β-barrels.[14–16] Their controlled transformation into rigid-rod quaternary β-structures with identical promise for structural and functional plasticity dramatically enriches the broad spectrum of applicability of rigid-rod molecules in bioorganic chemistry and beyond.

*Methods*

Spectroscopic studies: Absorption spectra were recorded on a Varian Cary 1 Bio spectrophotometer, circular dichroism spectra on a JASCO-710 spectropolarimeter, and fluorescence spectra on FluoroMax-2 (Jobin Yvon-Spex), all equipped with injector port, stirrer, and temperature controller (25 °C). Details on routine synthesis, purification (by reverse phase high-performance liquid chromatography (RP-HPLC)) and characterization of **2** will be reported elsewhere (see references [14–17]). Stock solutions were prepared from freshly repurified (RP-HPLC) **2**. An aliquot (usually 20 μL) of a concentrated stock solution in MeOH or dimethyl sulfoxide (DMSO) was added to buffer (usually 2 mL of 10 mM MES, pH as indicated; nearly identical results were obtained for < 100 mM MES, 10–100 mM phosphate, and < 100 mM XCl (X = Na, K)). Rigid-rod fibrils were characterized above the critical barrel concentration ($c(\mathbf{2}) = 3\ \mu M$) and below the appearance of minor ($c(\mathbf{2}) = 10\ \mu M$) to appreciable sample turbidity ($c(\mathbf{2}) = 15\ \mu M$). The binding of thioflavin T (ThT, usually 10 μM, Aldrich) was monitored by addition of an aliquot (usually 20 μL) from a concentrated stock solution in water to fibril samples prepared as above. UV/Vis: $\lambda_{max} = 412$ nm; CD: $\lambda_{max} = 420$ nm (Figure 3A); fluorescence emission: $\lambda_{ex} = 420$ nm, $\lambda_{em} = 500$ nm;[5] FRET: $\lambda_{ex} = 319$ nm,[14–16] $\lambda_{em} = 500$ nm. The following parameters were varied: $c(\mathrm{ThT}) = 0–14\ \mu M$ (see, for example, Figure 3A), $c(\mathbf{2}) = 0–25\ \mu M$ (see, for example, Figure 3B), pH 3.4–7.1 (e.g. Figure 3C), $c$(guanidinium chloride) = $c$(NaCl) = 0–2 M (*identical* decrease in intensities, not shown), $c(\mathrm{Cu(OAc)_2}) = 0 \rightarrow 90\ \mu M$ (decrease in intensities, not shown), $t = 5$ min–2 days (negligible change, not shown).

Atomic force microscopy (AFM): Samples were prepared as above and spectroscopically characterized prior to measurement. Barrels (see, for example, Figure 2) were prepared by deposition of 5 μL of an aqueous solution of **2** (1.5 μM, 1 mM MES, pH 5.5) on freshly cleaved mica followed by vibration isolated air-drying. Fibril self-assemblies (see, for example, Figure 5) were prepared by placing 5 μL of an aqueous solution of **2** (5 μM, 3.3 mM MES, pH 5.5) on graphite using otherwise identical procedures. Images were collected on a Nanoscope IIIa multimode scanning probe workstation (Digital Instruments) in tapping mode by using etched silicon tips (NanoProbes, Digital Instruments), a drive frequency of 250–300 kHz, and scanning speed at a line frequency of 1.2–2.2 Hz, at ambient temperature.

Negative-staining electron cryomicroscopy: Samples were prepared as above and spectroscopically characterized prior to measurement. Images were collected following routine protocols.[12, 19] In brief, 5 μL aqueous solutions of **2** (15–20 μM, 10 mM MES, pH 4.5–6.5, 0–90 μM $\mathrm{Cu(OAc)_2}$) were dropped on gold-sputtered 200-mesh carbon grids, placed upside down on a drop of saturated ammonium molybdate (10 s), blotted, vitrified with liquid ethane, mounted under liquid nitrogen, examined at ca. −172 °C (Philips CM12 electron microscope, 80 kV, nominal magnification 45 000), and recorded (Kodak 4489).

Received: May 29, 2001
Revised: September 9, 2001 [Z17195]

[1] J.-C. Rochet, P. T. Lansbury, Jr., *Curr. Opin. Struct. Biol.* **2000**, *10*, 60.
[2] J. W. Kelly, *Curr. Opin. Struct. Biol.* **1998**, *8*, 101.
[3] M. Fandrich, M. A. Fletcher, C. M. Dobson, *Nature* **2001**, *410*, 165.
[4] M. W. West, W. Wang, J. Patterson, J. D. Mancias, J. R. Beasley, M. H. Hecht, *Proc. Natl. Acad. Sci. USA* **1999**, *96*, 11211.
[5] Y. Takahashi, A. Ueno, H. Mihara, *ChemBioChem* **2001**, *2*, 75.
[6] H. A. Lashuel, S. R. LaBrenz, L. Woo, L. C. Serpell, J. W. Kelly, *J. Am. Chem. Soc.* **2000**, *122*, 5262.
[7] N. Yamada, K. Ariga, M. Naito, K. Matsubara, E. Koyama, *J. Am. Chem. Soc.* **1998**, *120*, 12192.
[8] T. S. Burkoth, T. L. S. Benzinger, D. N. M. Jones, K. Hallenga, S. C. Meredith, D. G. Lynn, *J. Am. Chem. Soc.* **1998**, *120*, 7655.
[9] T. S. Burkoth, T. L. S. Benzinger, V. Urban, D. M. Morgan, D. M. Gregory, P. Thiyagarajan, R. E. Botto, S. C. Meredith, D. G. Lynn, *J. Am. Chem. Soc.* **2000**, *122*, 7883.
[10] A. Lim, A. M. Makhov, M. J. Sanderholm, J. D. Griffith, B. W. Erikson, *Biochem. Biophys. Res. Commun.* **1999**, *264*, 498.

  1433-7851/01/4024-4660 $ 17.50+.50/0 

[11] C. Goldsbury, J. Kistler, U. Aebi, T. Arvinte, G. J. S. Cooper, *J. Mol. Biol.* **1999**, *285*, 33.
[12] B. Bohrmann, M. Adrian, J. Dubochet, P. Kuner, F. Müller, W. Huber, C. Nordstedt, H. Döbeli, *J. Struct. Biol.* **2000**, *130*, 232.
[13] H. Rapaport, K. Kjaer, T. R. Jensen, L. Leiserowitz, D. A. Tirrell, *J. Am. Chem. Soc.* **2000**, *122*, 12523.
[14] S. Matile, *Chem. Soc. Rev.* **2001**, *30*, 158.
[15] S. Matile, *Chem. Rec.* **2001**, *1*, 162.
[16] B. Baumeister, N. Sakai, S. Matile, unpublished results.
[17] B. Baumeister, A. Som, G. Das, N. Sakai, S. Matile, unpublished results.
[18] A. Engel, D. J. Müller, *Nat. Struct. Biol.* **2000**, *7*, 715.
[19] M. Adrian, J. Dubochet, S. D. Fuller, J. R. Harris, *Micron* **1998**, *29*, 145.

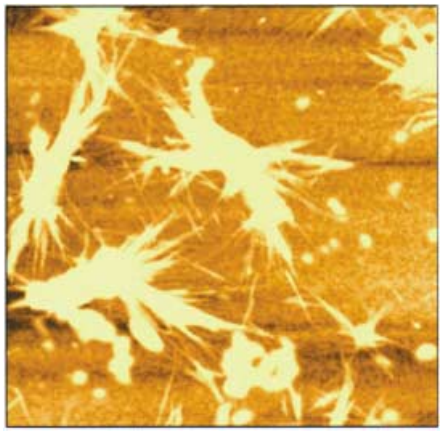

Figure 1. AFM image ($5 \times 5$ μm) of carbon nanotube stars on mica. The reaction mixture was directly cast on mica without any purification.

## Construction of Carbon Nanotube "Stars" with Dendrimers

Masahito Sano,* Ayumi Kamino, and Seiji Shinkai

Since carbon nanotubes are either metallic or semiconducting and exhibit ballistic transport,[1] the positioning of individual nanotubes in a well-defined spatial orientation may produce novel physical properties. By the currently available growth methods, carbon nanotubes are produced only in a stringlike form. Chemical modification is an attractive method for constructing various large-scale structures by positioning stringlike nanotubes. Herein we report the construction of star-shaped structures in which many carbon nanotubes radiate from a dendrimer center. These super-structured carbon nanotubes exhibit a peculiar response to electron beams. The synthesis of the stars was made possible by carefully fractionating the nanotubes by size.

Commercially available single-walled carbon nanotubes (SWNTs) are very long and are difficult to disperse in solution.[2–6] A standard procedure is to apply ultrasonication in strong acids to cut SWNTs into short pieces,[7, 8] followed by light etching to introduce oxygen-containing groups, such as carboxylic acids. Cut SWNTs are fractionated according to their characteristic sizes, as discussed herein. The carboxylic acid groups of the fractionated SWNTs were converted into acid chlorides and were then treated with the tenth generation poly(amidoamine) (PAMAM) starburst dendrimer (G10).

Atomic force microscopy (AFM) on cast films of the reaction mixture on mica reveals star-shaped objects (Figure 1). The average spine length is approximately 0.8 μm, which agrees well with the length of the SWNTs in the fraction. Although acid treatment tends to produce oxygen-containing groups at the side walls as well as at the ends,[9] our findings indicate, as proposed by other studies,[8, 10, 11] that the acid chloride groups at the open ends are more reactive than those at the side walls. Many spines are thicker than several nm and indicates, therefore, that there must be bundles of SWNTs in some burs. We think that many SWNTs simply adhere by van der Waals interactions to those tubes that have reacted with a dendrimer because of local high concentrations of tubes around the dendrimer. Some SWNTs are seen to bridge between two stars, which suggests that both ends of some SWNTs have reacted. Spectroscopic characterization was not possible because of the extremely low molar concentrations of stars that resulted from the initial low concentrations of SWNTs and difficulties in purification. Support that the SWNTs are covalently linked to the dendrimers rather than self-coagulated is provided by the observation that the star structures were completely destroyed after heating the stars for 3 h at 500 °C in $N_2$.

When the same sample shown in the AFM image of Figure 1 was coated with Pt/Pd and observed by scanning electron microscopy (SEM), star-shaped objects with much thicker burs were imaged. These spines were thicker than would be expected from the mere presence of the Pt/Pd films (Figure 2). Since the number of spines in the SEM image is smaller than that in the AFM image, it is likely that some of the spines in a star adhere together during residual water evaporation and metal deposition when they are placed in a vacuum. Without any metal coating, the acid-treated SWNTs

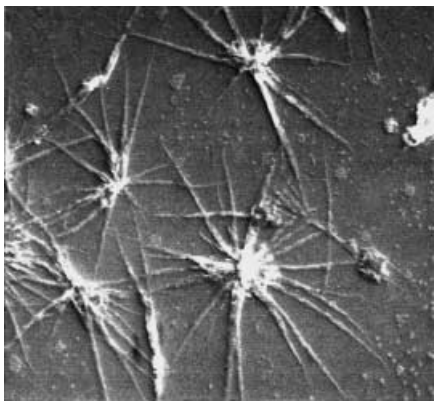

Figure 2. SEM image of the same sample as used to obtain Figure 1, but coated with Pt/Pd.

[*] Dr. M. Sano, A. Kamino, Prof. Dr. S. Shinkai
Chemotransfiguration Project—JST
2432 Aikawa, Kurume, Fukuoka 839-0861 (Japan)
Fax: (+81) 942-39-9012
E-mail: mass@jst.ktarn.or.jp

  1433-7851/01/4024-4661 $ 17.50+.50/0 